Available online at www.eccomasproceedia.org
Eccomas Proceedia COMPDYN (2025) 57- 68

ECCOMAS
Proceedia

COMPDYN 2025
10th ECCOMAS Thematic Conference on
Computational Methods in Structural Dynamics and Earthquake Engineering
M. Papadrakakis, M. Fragiadakis (eds.)
Rhodes Island, Greece, 15-18 June 2025

NUMERICAL MODELLING OF THE TRAFFIC INDUCED VIBRATION ON BRIDGES

Stefano Ercolessi[1], Carlo Rainieri[2], and Giovanni Fabbrocino[1,3]

[1]University of Molise
Via Francesco de Sanctis, Campobasso, Italy
e-mail: {stefano.ercolessi, giovanni.fabbrocino}@unimol.it

[2] Construction Technologies Institute, National Research Council of Italy
Naples, Italy
e-mail: rainieri@itc.cnr.it

[3] Construction Technologies Institute, National Research Council of Italy
L'Aquila, Italy
e-mail: fabbrocino@itc.cnr.it

Abstract. *Numerical modelling of Vehicle-Bridge Interaction is needed for advancing the understanding of bridge vibration levels and assess their safety. These simulations are complex, encompassing a wide range of influential factors, including traffic loads, environmental conditions, and roadway surface quality. Traffic loads introduce varying levels of operational stress on bridges, with a range of magnitudes and frequencies that could impact structural performance. Environmental factors, such as temperature fluctuations, wind forces, and seismic activity point out additional long-term challenges to structural integrity. Road surface roughness also plays a crucial role, affecting both vehicle performance and the structural health of bridges. By accurately integrating such variables into numerical simulations, it is possible predict and analyse the multifaceted interactions between vehicles and bridges under realistic operational scenarios. To incorporate, assess, and understand the impact of these phenomena on the mechanical behaviour of bridges, efficient simulation of bridge response is essential. In this paper, an approach to the numerical modelling of the problem is illustrated and discussed. A three-dimensional beam-based model incorporating the coupled bending-torsional response of bridges is introduced. On the other side, a simplified vehicle model, is coupled to the beam, based on the contact point paradigm. This numerical approach is employed to estimate the dynamic responses efficiently, bypassing the complexity of three-dimensional models that require detailed contact relations between subsystems. The flexibility and robustness of the framework are demonstrated through numerical validations.*

Keywords: Vehicle-Bridge Interaction, Finite Element Simulation, Bridge Traffic Induced Vibrations.

ISSN:2623-3347
Peer-review under responsibility of the organizing committee of COMPDYN 2025.
doi: 10.7712/120125.12657.25491

1 INTRODUCTION

The Vehicle-Bridge Interaction (VBI) phenomenon is a key aspect of the response of bridges under operational conditions. The investigation of this mechanical phenomenon has become increasingly significant owing to the continuous evolution of the automotive and heavy-vehicle industries, which has resulted in higher traffic volumes and greater load capacities for trucks. This evolution has been accompanied by significant progress in theoretical and numerical modelling techniques aimed at evaluating the effects of vehicles on bridges. Beam-based models have drawn interest due to their simplicity and computational efficiency while still providing acceptable levels of accuracy. The first studies on VBI date back to the 1850s [1, 2, 3] and mainly focused on the moving forces approach. The latter has been widely employed also for its ability to provide closed-form solutions to the equation of motion, which can be easily applied to various scenarios. However, it is limited by its inability to account for the inertial interaction between the two subsystems, namely, the bridge (principal system) and vehicles (secondary systems). To overcome this limitation, the moving mass approach was developed [4, 5], where forces are substituted by moving masses to obtain responses that include inertial interactions. Nevertheless, with the development of high-speed trains, a new methodology in which vehicles are represented using simplified dynamical models [6, 7, 8] has been increasingly adopted. These numerical models range from basic configurations, such as single sprung and unsprung-mass models [9, 10], to more complex representations, such as Quarter-Car (QC) [11] or half-car models [12], and even highly detailed models, such as tractor-trailers or complete three-dimensional vehicle models coupled with bi- or three-dimensional bridge models [13, 14]. However, increasing the level of detail in both the principal and secondary system models results in a significant impact on the computational efforts and, consequently, on the capability to perform numerical simulations where a large number of vehicles are considered. Hence, it is impractical to simulate a real traffic scenario with realistic traffic volume. Furthermore, traditional beam-based models typically focus only on the flexural response along the vertical axis, neglecting real bridge dynamics under traffic excitation. Bridge cross-sections are usually mono-symmetric and are characterized by a flexural-torsional mechanism, which is activated by the eccentricity of the vehicle loads. Given these foundations, the present study aims to introduce a numerical beam-based framework for VBI simulation and to address the aforementioned limitations by defining a finite element beam with seven degrees of freedom and its coupling mechanism with moving QCs. This element accounts for the shear deformability [15], rotary inertia, and uniform and non-uniform torsion[16]. Additionally, it is capable of capturing the effects of flexural-torsional coupling mechanisms that arise from typical nonsymmetrical cross-sections. The proposed framework also includes a coupling mechanism between the developed beam finite element and QC models moving at a constant velocity along the beam. To validate the proposed approach, the numerical results were compared with those obtained from a comprehensive three-dimensional model created using the well-established commercial finite element software Abaqus 2024 (hereafter referred to as Abaqus). The validation process demonstrated that the proposed framework captured the global response of the bridge structure under the effect of more than one moving QC. Moreover, it highlights that the local effects induced by contact enforcement in the three-dimensional models have a minimal impact on the overall structural response for the vehicles tested.

2 BEAM BASED VBI FINITE ELEMENT FRAMEWORK

In the following section, a brief introduction to the beam-based VBI model is presented. Two are the main topics hereafter presented: the seven degrees-of-freedom beam finite element used for VBI simulations, and its coupling mechanism with constant-velocity moving QCs. The main purpose was to define a finite element methodology focused on VBI simulations, which can be easily implemented to generate and simulate the dynamic responses of bridge structures subjected to vehicular traffic. The principal system is modelled by considering a beam finite element that includes shear deformation [15], rotary inertia, and uniform and non-uniform torsion. The presence of a non-uniform torsional mechanism entails the introduction of the Vlasov theory [16], which must be combined with the presence of shear contribution and rotary inertial effects in the definition of the beam response. Moreover, the coupling flexural-torsional mechanism due to the nonsymmetrical features of the commonly employed cross sections is included in the finite element formulations. Thereafter, the coupling mechanism between the principal system and moving QCs models based on Yang's assumption [17] is presented.

2.1 Finite element beam formulation

The beam finite element formulation refers to a generic section, as illustrated in Figure 1, where the cross section is identified with its midline. Reference system is assumed in correspondence of the elastic center of the beam cross section, and P(y_p, z_p) identifies its shear center. A theoretical procedure to define the finite-element formulation for the beam problem is illustrated.

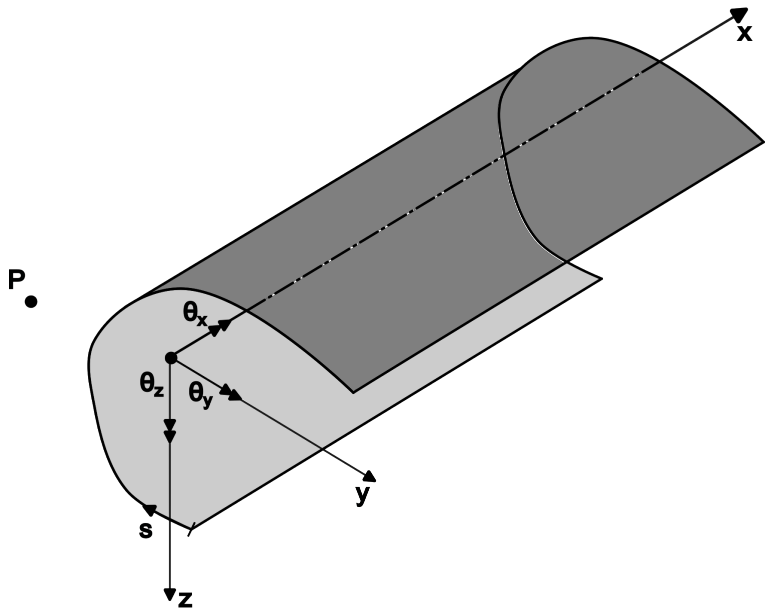

Figure 1: Generic beam cross-section and associated reference system.

The system of coupled partial differential equations, which represents the strong form of the equations of motion can be written for the analysed degrees of freedom as

$$\begin{aligned}
GA_y \cdot (w_{y,x} - \theta_z)_{,x} - \rho A \cdot w_{y,tt} + \rho S_{ys} \cdot \theta_{x,tt} + q_y = 0 \\
EI_z \cdot \theta_{z,xx} + GA_y \cdot (w_{y,x} - \theta_z) - EI_{yz} \cdot \theta_{y,xx} + EI_{\omega z} \cdot \theta_{x,xxx} \\
-\rho I_z \cdot \theta_{z,tt} - \rho I_{\omega z} \cdot \theta_{x,xtt} + \rho I_{yz} \cdot \theta_{y,tt} + m_z = 0
\end{aligned} \tag{1}$$

$$\begin{aligned}
GA_z \cdot (w_{z,x} + \theta_y)_{,x} - \rho A \cdot w_{z,tt} - \rho S_{zs} \cdot \theta_{x,tt} + q_z = 0 \\
EI_y \cdot \theta_{y,xx} - GA_z \cdot (w_{z,x} + \theta_z) - EI_{yz} \cdot \theta_{z,xx} - EI_{\omega y} \cdot \theta_{x,xxx} \\
-\rho I_y \cdot \theta_{y,tt} + \rho I_{\omega y} \cdot \theta_{x,xtt} + \rho I_{yz} \cdot \theta_{z,tt} + m_y = 0
\end{aligned} \tag{2}$$

$$\begin{aligned}
GJ \cdot \theta_{x,xx} - \rho I_p \cdot \theta_{x,tt} + \rho S_{ys} \cdot w_{y,tt} - \rho S_{zs} \cdot w_{z,tt} + m_x = 0 \\
EI_\omega \cdot \theta_{x,xxx} + EI_{\omega z} \cdot \theta_{z,xx} - EI_{\omega y} \cdot \theta_{y,xx} - \rho I_\omega \theta_{x,xtt} \\
-\rho I_{\omega z} \cdot \theta_{z,tt} + \rho I_{\omega y} \cdot \theta_{y,tt} + b_x = 0
\end{aligned} \tag{3}$$

In Eqs. (1–3), $w_i(x,t)$, where $i = x, y, z$ are the total displacement components of the cross-section and θ_i are the rotation counterparts. Moreover, $(_{,x})$ and $(_{,t})$ indicate respectively the derivatives with respect to the coordinate x and time t. The constants E and G denote the elasticity and tangential moduli of the linear elastic material, respectively. Furthermore, the first and the second order moments of the generic cross-section are

$$S_{zs} = \int_A (y - y_P) dA \quad S_{ys} = \int_A (z - z_P) dA \tag{4}$$

$$\begin{aligned}
I_z = \int_A z^2 dA \quad I_y = \int_A y^2 dA \quad I_{yz} = \int_A yz\, dA \\
I_{\omega z} = \int_A \omega y\, dA \quad I_{\omega y} = \int_A \omega z\, dA \quad I_\omega = \int_A \omega^2 dA
\end{aligned} \tag{5}$$

where $\omega(s)$ is the so-called warping function and s is curvilinear abscissa of the cross-section considered positive in counter-clockwise direction. Furthermore, the torsional parameter J and the polar moment of inertia I_P are defined as follow

$$\begin{aligned}
J = \int_A \left\{ \left[(y - y_p) + \omega_{,z} \right]^2 + \left[(z - z_p) - \omega_{,y} \right]^2 \right\} dA \\
I_p = \int_A \left[(y - y_p)^2 + (z - z_p)^2 \right] dA
\end{aligned} \tag{6}$$

q_i and m_i, with $i = x, y, z$ are respectively the distributed loads and moments, and b_x is the bi-moment in accordance with the selected reference system (c.f. Eqs. (1-3)). Hence, integrating by part the system of partial differential equations representing the strong form of the equation of motion, and multiplying each contributions by a test function $\mathcal{H}_i$, adequately chosen to coincide, after, with the desired shape functions $\mathcal{N}_i$, it is possible to find the finite element formulation according to the standard Galerkin approach [18]

$$GA_y \int_0^L \mathcal{H}_{1,x} \cdot (w_{y,x} - \theta_z)dx + \rho A \int_0^L \mathcal{H}_1 \cdot w_{y,tt}dx - \rho S_{ys} \int_0^L \mathcal{H}_1 \cdot \theta_{x,tt}dx \qquad (7)$$
$$- \int_0^L \mathcal{H}_2 \cdot q_y dx = 0$$
$$EI_z \int_0^L \mathcal{H}_{2,x} \cdot \theta_{z,x}dx - GA_y \int_0^L \mathcal{H}_2 \cdot (w_{y,x} - \theta_z)dx - EI_{yz} \int_0^L \mathcal{H}_{2,x} \cdot \theta_{y,x}dx$$
$$+EI_{\omega z} \int_0^L \mathcal{H}_{2,x} \cdot \theta_{x,xx}dx + \rho I_z \int_0^L \mathcal{H}_2 \cdot \theta_{z,tt} + \rho I_{\omega z} \int_0^L \mathcal{H}_2 \cdot \theta_{x,xtt}dx$$
$$-\rho I_{yz} \int_0^L \mathcal{H}_2 \cdot \theta_{y,tt}dx - \int_0^L \mathcal{H}_2 \cdot m_z dx = 0$$

$$GA_z \int_0^L \mathcal{H}_{3,x} \cdot (w_{z,x} + \theta_y)dx + \rho A \int_0^L \mathcal{H}_3 \cdot w_{z,tt}dx + \rho S_{zs} \int_0^L \mathcal{H}_3 \cdot \theta_{x,tt}dx \qquad (8)$$
$$- \int_0^L \mathcal{H}_3 \cdot q_z dx = 0$$
$$EI_y \int_0^L \mathcal{H}_{4,x} \cdot \theta_{y,x}dx + GA_z \int_0^L \mathcal{H}_4 \cdot (w_{z,x} + \theta_y)dx - EI_{yz} \int_0^L \mathcal{H}_{4,x} \cdot \theta_{z,x}dx$$
$$-EI_{\omega y} \int_0^L \mathcal{H}_{4,x} \cdot \theta_{x,xx}dx + \rho I_y \int_0^L \mathcal{H}_4 \cdot \theta_{y,tt} - \rho I_{\omega y} \int_0^L \mathcal{H}_4 \cdot \theta_{x,xtt}dx$$
$$-\rho I_{yz} \int_0^L \mathcal{H}_4 \cdot \theta_{z,tt}dx - \int_0^L \mathcal{H}_4 \cdot m_y dx = 0$$

$$GJ \int_0^L \mathcal{H}_{5,x} \cdot \theta_{x,x}dx + \rho I_p \int_0^L \mathcal{H}_5 \cdot \theta_{x,xtt}dx + \rho S_{zs} \int_0^L \mathcal{H}_5 \cdot w_{z,tt}dx \qquad (9)$$
$$-\rho S_{ys} \int_0^L \mathcal{H}_5 \cdot w_{y,tt}dx - \int_0^L \mathcal{H}_5 \cdot m_x dx = 0$$
$$EI_\omega \int_0^L \mathcal{H}_{5,xx} \cdot \theta_{x,xx}dx + EI_{\omega z} \int_0^L \mathcal{H}_{5,xx} \cdot \theta_{z,x}dx - EI_{\omega y} \int_0^L \mathcal{H}_{5,xx} \cdot \theta_{y,x}dx$$
$$+\rho I_\omega \int_0^L \mathcal{H}_{5,x} \cdot \theta_{x,xtt}dx + \rho I_{\omega z} \int_0^L \mathcal{H}_{5,x} \cdot \theta_{z,tt}dx$$
$$-\rho I_{\omega y} \int_0^L \mathcal{H}_{5,x} \cdot \theta_{y,tt}dx - \int_0^L \mathcal{H}_{5,x} \cdot b_x dx = 0$$

substituting in Eqs. (7-9) the approximation for the displacement field

$$w_y(x,t) = \mathbf{N}_1(x)\mathbf{d}_1(t); \quad \theta_z(x,t) = \mathbf{N}_2(x)\mathbf{d}_1(t); \quad w_z(x,t) = \mathbf{N}_3(x)\mathbf{d}_2(t); \qquad (10)$$
$$w_z(x,t) = \mathbf{N}_4(x)\mathbf{d}_2(t); \quad w_y(x,t) = \mathbf{N}_5(x)\mathbf{d}_3(t);$$

and the test functions with the shape functions $\mathbf{N}_i$, the consistent mass matrix $\mathbf{M}$, the stiffness matrix $\mathbf{K}$ and the force vector $\mathbf{f}$ are derived respectively from the kinetic energy, strain potential energy and the external work terms. In Eq.10 the vector $\mathbf{d}_i$ is the associated column vectors which holds the associated degrees of freedom.

2.2 Beam-QCs coupling mechanism

After defining the finite element formulation for the beam element, the coupling procedure between the i-th QC model and beam element must be addressed. In this context, the Yang assumption of perfect contact [17] is integrated to account for the flexural-torsional mechanism. The ith QC model (cf., Figure 2a) is modelled by two masses, an upper m_{vi} and a lower mass m_{wi}, linked by a spring-dashpot device, characterized by a stiffness constant k_{vi} and a damping coefficient c_{vi}. The QCs move at a constant speed v_i and a fixed horizontal distance h_i from the longitudinal axis of the bridge. Moreover, the road roughness, denoted as $r_i(x)$, can be simulated according to the well-established procedure reported in standard ISO-8608 [19]. The i-th QC and the principal system are in contact by means of the so-called contact point, identified by the spatial coordinate $x_{ci}(t)$ (c.f. Figure 2b).

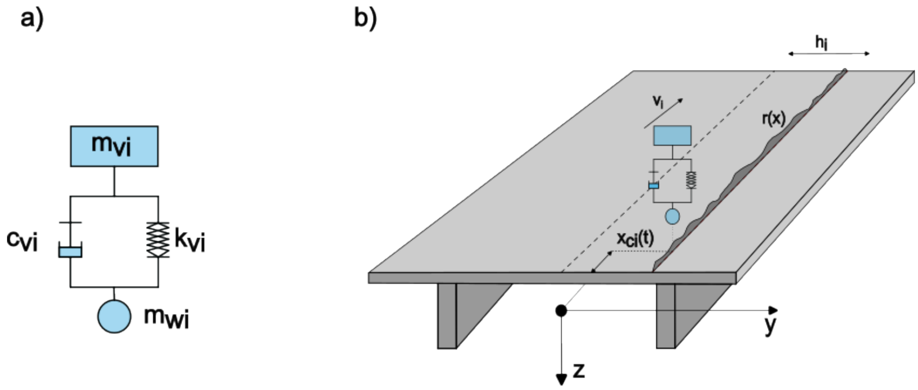

Figure 2: Graphical representation of the QC model (a) and of the QC and the bridge system (b).

The equation of motion of the i-th QC along the vertical degree of freedom and the physical definition of the contact force f_{ci} can defined considering a free body diagram of the QC and expressed as

$$
\begin{aligned}
m_{vi}u_{vi,tt} + c_v(u_{vi,t} - u_{wi,t} - r_{i,t}) + k_v(u_{vi} - u_{wi} - r_i) = 0 \\
f_{ci} = m_{wi}u_{wi,tt} - c_{vi}(u_{vi,t} - u_{wi,t} - r_{i,t}) - k_{vi}(u_{vi} - u_{wi} - r_i)
\end{aligned} \tag{11}
$$

Because of the perfect contact hypothesis described in Eq. (11b), it is possible to couple the two subsystems corresponding to the j-th finite element of the beam, which is identified by $x_{ci}(t)$. Moreover, due to the capability of the beam element to account for the torsional responses, in the hypothesis of small displacements it is possible to compute the total vertical displacement of a generic point of the cross-section as

$$
u_{wi} = w_z(x_{ci}) - h_i \cdot tan[\theta_x(x_{ci})] \approx w_z(x_{ci}) - h_i \cdot \theta_x(x_{ci}) \tag{12}
$$

Where $tan()$ represents the trigonometric tangent function. The condition pointed out by Eq. (12) can be integrated in the finite element framework considering the vertical displacement of the lower mass u_{wi} and the beam point in correspondence of $x_{ci}(t)$. Hence,

$$
u_{wi} = \mathbf{N}(x_c)\mathbf{G}\mathbf{d}_b = \bar{\mathbf{N}}_i\mathbf{d}_b \tag{13}
$$

where, $\mathbf{d}_b$ is the column vector, which stores the n degrees of freedom of the bridge, $\mathbf{N}(x_c)$ is the global shape function row vector and $\mathbf{G}$ is n-th order square matrix defined as

$$\mathbf{G} = \mathbf{e}_i \otimes \mathbf{e}_i - \tilde{\mathbf{e}}_i \otimes \tilde{\mathbf{e}}_i \tag{14}$$

In Eq. (14), $\mathbf{e}_i$ is the column vector which holds zeros in each position except for the indices associated with the active finite element, which is identified by $x_{ci}(t)$ and $\tilde{\mathbf{e}}_i$ is the torsional counterpart. Deriving with respect to time Eq.(13) and substituting in Eq. (11b) the contact force of the i-th QC can be expressed as

$$\begin{aligned} f_{ci} = m_{wi}(v_i^2\bar{\mathbf{N}}_{i,xx}\mathbf{d}_b + 2v_i\bar{\mathbf{N}}_{i,x}\mathbf{d}_{b,t} + \bar{\mathbf{N}}_i\mathbf{d}_{b,tt}) + c_{vi}(v_i\bar{\mathbf{N}}_{i,x}\mathbf{d}_b + \bar{\mathbf{N}}_i\mathbf{d}_{b,t}) \\ + k_{vi}\bar{\mathbf{N}}_i\mathbf{d}_b - c_{vi}(u_{vi,t} - v_i \cdot r_{i,x}) - k_{vi}(u_{vi} - r_i) \end{aligned} \tag{15}$$

Once, that the formulations associated with the dynamic of the beam element and i-th QC are obtained it is possible to couple the two sub-system via the contact forces f_{ci}, the equation of motion of the principal system can be re-casted in matrix notation as

$$\mathbf{M}_b\mathbf{d}_{b,tt} + \mathbf{C}_b\mathbf{d}_{b,t} + \mathbf{K}_b\mathbf{d}_b = \sum_{i=1}^{q} \bar{\mathbf{N}}_i^T[g(m_{wi} + m_{vi}) - f_{ci}] \tag{16}$$

where g in the force vector indicates the acceleration of gravity. $\mathbf{M}_b$, $\mathbf{C}_b$ and $\mathbf{K}_b$ denote the bridge mass, damping, and stiffness matrices, respectively. The damping matrix, even though it is not defined, is intended by considering the proportional damping approach and derived from the mass and stiffness matrix. q is the total number of QCs considered in the analysis. The coupled response of the bridge is obtained substituting Eq.(15) in Eq. (16)

$$\begin{aligned} \left(\mathbf{M}_b + \sum_{i=1}^{q} m_{wi}\bar{\mathbf{N}}_i^T\bar{\mathbf{N}}_i\right)\mathbf{d}_{b,tt} + \left[\mathbf{C}_b + \left(\sum_{i=1}^{q} 2v_i m_{wi}\bar{\mathbf{N}}_i^T\bar{\mathbf{N}}_{i,x} + c_{vi}\bar{\mathbf{N}}_i^T\bar{\mathbf{N}}_i\right)\right]\mathbf{d}_{b,t} \\ + \left[\mathbf{K} + \left(\sum_{i=1}^{q} v_i^2 m_{wi}\bar{\mathbf{N}}_i^T\bar{\mathbf{N}}_{i,xx} + v_i c_{vi}\bar{\mathbf{N}}_i^T\bar{\mathbf{N}}_{i,x} + k_{vi}\bar{\mathbf{N}}_i^T\bar{\mathbf{N}}_i\right)\right]\mathbf{d}_b \\ = \sum_{i=1}^{q} \bar{\mathbf{N}}_i^T\left[g(m_{wi} + m_{vi}) + c_{vi}(u_{vi,t} - v_i \cdot r_{i,x}) + k_{vi}(u_{vi} - r_i)\right] \end{aligned} \tag{17}$$

The differential equations associated to the i-th QC are composed substituting Eq.(13) and its first and second derivatives with respect to time in the equation of motion (c.f. Eq. 11a)

$$m_{vi,tt}u_{vi,tt} + c_{vi}u_{vi,t} + k_{vi}u_{vi} = c_{vi}\left(v_i\bar{\mathbf{N}}_{i,x}\mathbf{d}_b + \bar{\mathbf{N}}_i\mathbf{d}_{b,t} + v_i r_{i,x}\right) + k_{vi}\left(\bar{\mathbf{N}}_i\mathbf{d}_b + r_i\right) \tag{18}$$

Finally, Eq. (17) and Eq. (18) can be re-casted in matrix notation as

$$\begin{bmatrix} \mathbf{M}_{vv} & 0 \\ 0 & \mathbf{M}_{bb} \end{bmatrix}\begin{Bmatrix} \mathbf{u}_{v,tt} \\ \mathbf{u}_{b,tt} \end{Bmatrix} + \begin{bmatrix} \mathbf{C}_{vv} & \mathbf{C}_{vb} \\ \mathbf{C}_{bv} & \mathbf{C}_{bb} \end{bmatrix}\begin{Bmatrix} \mathbf{u}_{v,t} \\ \mathbf{u}_{b,t} \end{Bmatrix} + \begin{bmatrix} \mathbf{K}_{vv} & \mathbf{K}_{vb} \\ \mathbf{K}_{bv} & \mathbf{K}_{bb} \end{bmatrix}\begin{Bmatrix} \mathbf{u}_v \\ \mathbf{u}_b \end{Bmatrix} = \begin{Bmatrix} \mathbf{f}_v \\ \mathbf{f}_b \end{Bmatrix} \tag{19}$$

In Eq. (19) the quantities associated with the terms $(_{vv})$ or $(_v)$ are the terms associated with vehicles, $(_{bb})$ or $(_b)$ with the bridge and others are the mixed terms.

3 FINITE ELEMENT VALIDATION OF THE VBI FRAMEWORK

The finite element validation of the approach presented in Section 2 is reported below. Dynamic responses were computed by referring to custom-coded C++ software and compared with those obtained by a three-dimensional model carried out in Abaqus. The double-tee section is considered to be a bridge structure (cf. Figure 3).

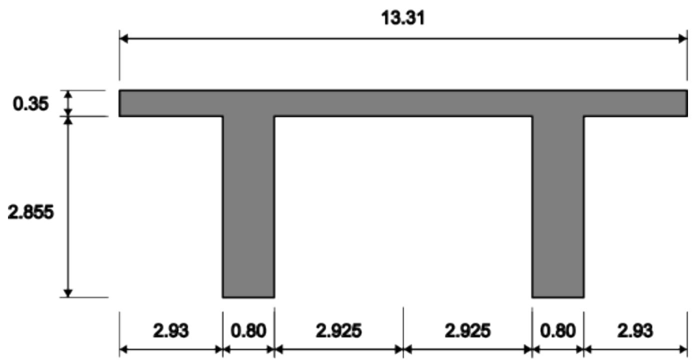

Figure 3: Graphical representation of the double-tee beam.

The material is considered to be linear elastic with the mechanical characteristics reported in Table 3. From Abaqus, the structure, which is intended to be 40 m long, was modelled using 197440 C3D8R brick elements. The boundary conditions are enforced at the beam ends, restraining a reference point, positioned in the elastic center of the section, and kinematically coupled with the nodes of the beam end surface. Three translational degrees of freedom and torsional rotation were constrained. The kinematic constraint also imposed a constraint on the warping of the two ends.

Description	Parameter		Unit
Elastic modulus	E	33000.00	MPa
Shear modulus	G	13750.00	MPa
Poisson coefficient	ν	0.20	–
Density	ρ	2500.00	kg/m^3

Table 1: Material mechanical properties.

The two QC models considered moving at a constant speed v_i of 4 m/s^2 on the bridge, with the same horizontal deviation from the longitudinal axis of the beam h_i of 3.325 m and a mutual distance of 30 m. The mechanical characteristics of the two QCs are listed in Table 3 where QC-1 is the first QC that enters the beam. The QCs are modelled in Abaqus referring to contact relations, where the upper surface of the bridge deck is the main surface and the lower mass interacts with it, enforcing frictionless tangential behavior and hard contact in the normal direction.

The monitored responses are the displacement time histories corresponding to the three nodes of the midspan cross section: (i) Node 1 at $z = 0$ m, (ii) Node 2 at $z = 6.655$ m, and (iii) Node 3 at $z = h_i$. The vertical responses obtained from the Abaqus model were compared to those retrieved by the proposed model using Eq. (12).

		QC-1		QC-2	
Upper mass	m_{v1}	1000.00	m_{v2}	2000.00	kg
Damping coefficient	c_{v1}	5026.55	c_{v2}	10053.10	kNs/m
Stiffness coefficient	k_{v1}	39478.40	k_{v2}	78956.80	kN/m

Table 2: Mechanical parameters of QC-1 and QC-2 employed in numerical simulations.

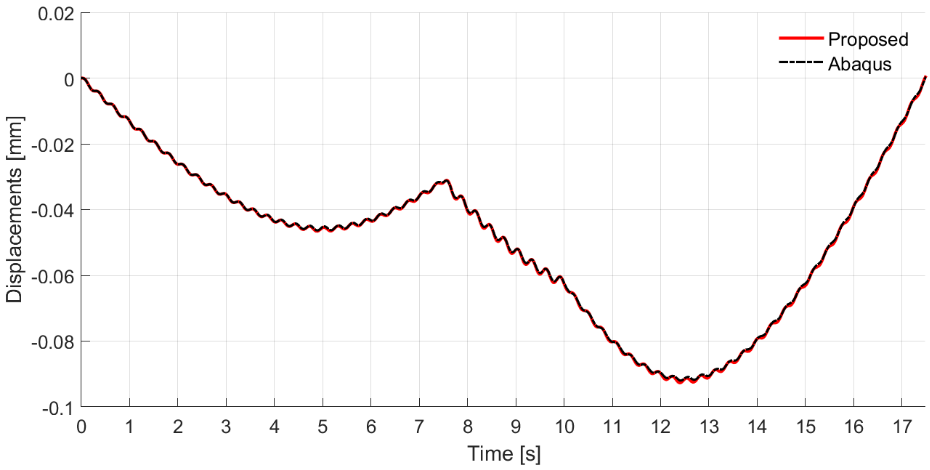

Figure 4: Node 1 displacements responses Abaqus (dashed black line) Vs proposed (red line).

These quantities are shown in Figures 4–6. In particular, from the displacement responses, the impact and the influence of both the QCs entering the structure are clearly observable, with maximum effects measured in correspondence of the QC passing on the beam mid-section. Moreover, it is also possible to observe how the different masses of the QC models impact the displacements corresponding to a major amplitude for QC-2 in the analysis. A comparison of the two responses indicates good agreement between the two procedures for Node 1 and Node 2, respectively (Figure 4 and Figure 5. Moreover, it is interesting to analyze the effects of Node 3 (c.f., Figure 6), where the contact relations in the three-dimensional model introduce local effects in correspondence of the contact-point. Indeed, the responses from the Abaqus perspective seem to be affected by some local effects, as evidenced by an increase in the vertical displacements and clear peaks at the exact instant when the examined cross-section is in contact with a QC. However, these local effects are localized in both space and time, and even though the proposed beam-based method is not capable of reproducing them, they do not affect the overall accuracy of the proposed method, which is in accordance with the beam-based methodologies aimed at obtaining an accurate global response of the structure. Furthermore, the significant discrepancy in the number of finite elements adopted by the two formulations is a clear advantage of the proposed approach, as it enables numerical simulations of structures, even under high traffic volumes, offering significant benefits in terms of computational resources.

4 CONCLUSIONS

The present work describes a beam-based finite-element framework aimed at performing numerical simulations of the VBI phenomenon. Both the main and secondary systems are idealized and modelled with the aim of limiting the total number of degrees of freedom while

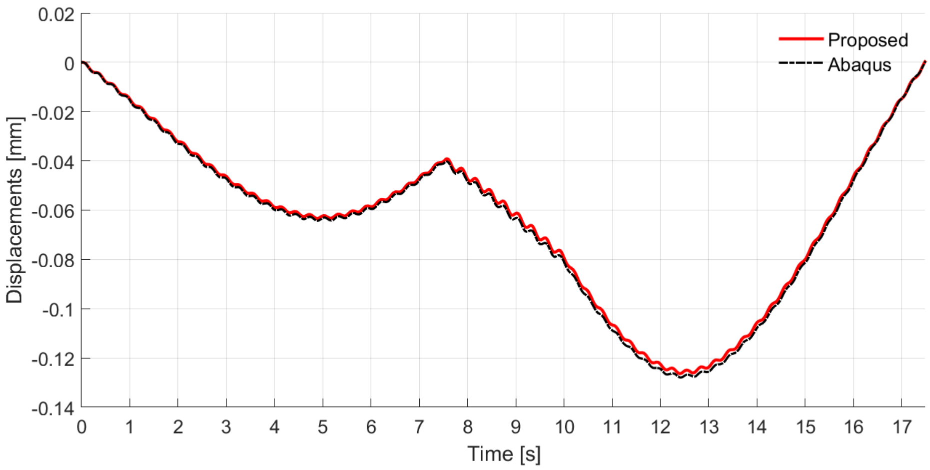

Figure 5: Node 2 displacements responses Abaqus (dashed black line) Vs proposed (red line).

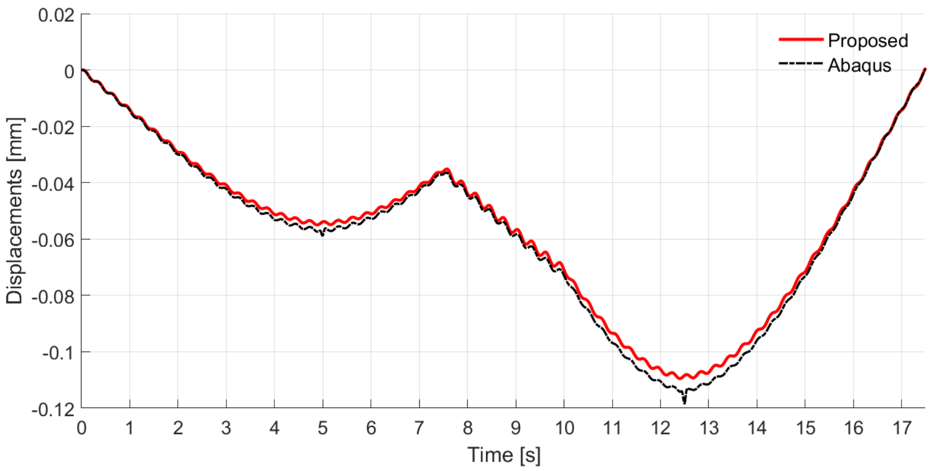

Figure 6: Node 3 displacements responses Abaqus (dashed black line) Vs proposed (red line).

maintaining good accuracy with respect to more complex models. A beam finite element capable of accounting for shear deformability, rotary inertia, and uniform and non-uniform torsion was presented. The presence of such mechanisms in the principal system enhances the three-dimensional performance of beam-based methods for VBI analysis. The vehicles were discretized as QC models moving at a constant speed on the beam. The presented coupling formulation between the principal and secondary systems is based on the perfect contact hypothesis, which is extended to account for the eccentricity of moving vehicles. Moreover, the presented framework was validated against a complete three-dimensional finite element model realized in Abaqus, a well-established commercial finite element software, where the coupling mechanism between two systems relies on classical contact relations. The results obtained from the numerical comparison confirmed that beam-based models in the presence of torsional behavior can adequately describe the overall response of the bridges, at least in their elastic regime, for VBI phenomena. Nevertheless, the local effects highlighted in the previous section, essentially owing to the detailed description of the three-dimensional model, are localized in the neighborhood of the contact area and do not significantly impact the overall response of the finite element representation. Furthermore, the large difference in terms of the finite element employed in the discretization results in a computationally advantageous approach, especially in models with a significant number of moving QCs, as in the case of high traffic volumes.

5 ACKNOWLEDGEMENTS

Activity carried out in the framework of NATIONAL RECOVERY AND RESILIENCE PLAN (PNRR) Mission 4 “Education and Research” - Component C2 Investment 1.1, “Fund for the National Research Program and Projects of Relevant National Interest (PRIN)” Project PRIN PNRR 2022 Vibration Serviceability Of Road bridges (ViSOR), code P2022KAEWY.

REFERENCES

[1] D. Galton, Report of the commissioners appointed to inquire into the application of iron to railway structures. *J Franklin Inst* , **49**, 289-302, 1850.

[2] S.P. Timoshenko. On the forced vibrations of bridges. *The London, Edinburgh, and Dublin Philosophical Magazine and Journal of Science*, **43**, 1922.

[3] L. Frýba. Non-stationary response of a beam to a moving random force. *J Sound Vib*, **46**, 1976.

[4] A.O. Cifuentes. Dynamic response of a beam excited by a moving mass. *Finite Elements in Analysis and Design* , **5**, 1989.

[5] M. Dehestani, M. Mofid, A. Vafai. Investigation of critical influential speed for moving mass problems on beams. *Appl Math Model*, **33**, 2009.

[6] Y.B. Yang, B.H. Lin. Vehicle-Bridge Interaction Analysis by Dynamic Condensation Method, *Journal of Structural Engineering*, **121**, 1995.

[7] L. Kwasniewski, H. Li, J. Wekezer, J. Malachowski. Finite element analysis of vehicle-bridge interaction. *Finite Elements in Analysis and Design*, **42**, 2006.

[8] C.D. Stoura, E.G. Dimitrakopoulos. Additional damping effect on bridges because of vehicle-bridge interaction. *J Sound Vib*, **476**, 2020.

[9] T. Dahlberg. Vehicle-Bridge Interaction. *Vehicle System Dynamics*, **13**, 187-206, 1984.

[10] P.K. Chatterjee, T.K. Datta, C.S. Surana. Vibration of Suspension Bridges under Vehicular Movement. *Journal of Structural Engineering*, **120**, 1994.

[11] S. Ercolessi, G.Fabbrocino, C.Rainieri. Indirect measurements of bridge vibrations as an experimental tool supporting periodic inspections. *Infrastructures*, **6**, 2021.

[12] S.H. Ju, H.T. Lin. A finite element model of vehicle-bridge interaction considering braking and acceleration.*J Sound Vib*, **303**, 2007.

[13] Q. Xie, W. Han, Y. Yuan. Refined Vehicle-Bridge Interaction Analysis Using Incompatible Solid Finite Element for Evaluating Stresses and Impact Factors. *Advances in Civil Engineering*, **1**, 2020.

[14] S. Mei, C. Caprani, D. Cantero. Dynamic amplification of multi-span simply-supported prestressed concrete girder viaducts subjected to multi-body heavy vehicles. *Structures*, **55**, 2023.

[15] S.P. Timoshenko, X. On the transverse vibrations of bars of uniform cross-section. *The London, Edinburgh, and Dublin Philosophical Magazine and Journal of Science*, **43**, 125-131, 1922.

[16] V. Vlasov, *Thin-walled elastic beam, 2nd Ed.* Israel Program for Scientific Translation, 1961.

[17] Y.B. Yang, J.D. Yau, Vehicle-Bridge Interaction Element for Dynamic Analysis. *Journal of Structural Engineering*, **123**, 1997.

[18] K.J. Bathe, *Finite Element Procedures*, 1996.

[19] P.Múčka, Simulated road profiles according to ISO 8608 in vibration analysis. *J Test Eval*,**46**,2018.